ISSN: 2634 - 8845

Journal of Earth and Environmental Science Research

SCIENTIFIC Research and Community

Review Article

Open Access

Migmatite-Gneiss-Granite Basement of Southwestern Nigeria: Mineralogical and Geochemical Evidence for a Possible Common Ancient Protolith

Olusola A OlaOlorun* and Oluwatoyin O Akinola

Department of Geology, Ekiti State University, PMB 5363, Ado-Ekiti, Nigeria

ABSTRACT

Nigeria occupies southern section of the Pan-African orogenic belt and migmatite-gneiss-granite terrain forms a major component of its basement complex. Field geology, optical mineralogy and geochemical study of this rock unit in Idanre area, SW Nigeria were undertaken with a view to characterize them, elucidate their tectonic significance, and determine their origin. Major, trace and Rare Earth Elements (REE) composition were determined by XRF and ICP-MS techniques respectively in Bureau Veritas, Vancouver, Canada. Field geology reveals the granite which occur in three textural types (fine-grained (OGf), porphyritic (OGp), and coarse-grained undifferentiated OGu) intrudes the low-lying migmatite-gneiss complex. The country rock comprises of aggregation of migmatite, biotite-hornblende gneiss and banded gneiss sub-units which bear pervasive tectonic signatures of polymetamorphic and orogenic activities. Optical results reveal the migmatite-gneiss country rock comprise of quartz, feldspar and biotite with granoblastic to porphyroblastic texture. The granitoids contain interlocks of quartz, K-feldspar, microcline, biotite, hornblende and accessory magnetite, and sphene. Large hornblende crystals in the coarse-grained granite are poikilitic while the porphyritic type contains myrmekite. The decreasing trends of Harker diagrams with respect to SiO_2 indicates crystal fractionation. $FeO^t/(FeO^t+MgO)$ versus SiO_2 plot classifies the gneiss as ferroan type, Al_2O_3 versus MgO plot classifies it as orthogneiss, total alkali (Na_2O+K_2O) versus SiO2 (TAS) classified the rocks as granite. K_2O versus SiO_2 diagram classifies the rocks as continental granophyre. AFM [(Na2O+K2O)-Fe_2O_3-MgO] ternary diagram suggests the rocks are calc-alkaline, while ternary plot of Ba-Rb-Sr classifies the rock as anomalous granite. Diagram of $Al_2O_3+Na_2O+K_2O$ versus Alumina Saturation Index (ANK vs ASI) indicates ASI<1.0 showing the granite is metaluminous. R1 versus R2 diagram indicate the rocks are largely late orogenic, La/Sm versus Sm diagram suggest that partial melting play a significant role in the magma source. A consistently low ACNK (<1.1) value, a decreasing trend on ACNK versus SiO_2 diagram indicates the rocks originated from anatectic melt of igneous protoliths. The similar shape of the chondrite normalized REE distribution pattern for both the migmatite-gneiss and granite indicate similar geochemical trends which possibly connote common ancient igneous protolith.

***Corresponding author**

Olusola A OlaOlorun, Department of Geology, Ekiti State University, PMB 5363, Ado-Ekiti, Nigeria.

Received: June 14, 2024; **Accepted:** June 17, 2024; **Published:** July 05, 2024

Keywords: SW Nigeria, Migmatite-Gneiss-Granite Terrain, Porphyroblastic, Co-Magmatic, Igneous Protolith

Introduction

A greater percentage of continental crust of Archean-Proterozoic age around the world have been subsequently recycled and mixed with younger crust by orogenic processes. This is particularly true in orogenic belts; shear, rift and subduction zones where plates converge and interact [1-9]. The exact character of these ancient crust remains uncertain because the primary properties and origin of most Precambrian protoliths are obscured to varying degrees by multiple overprints of deformation, partial melting and recrystallization [10]. Archaean terrains has been through tectono-magmatic and metamorphic activities during Neoproterozoic to earliest Paleozoic. The tectono-thermal activity of 500 Ma ago saw the formation of many mobile belts around older cratons in Africa [11]. During this time, Nigeria like many other parts of Africa witnessed widespread magmatic activities which culminated in the emplacement of granites into the older gneissic basement. Such regions are now characterized by migmatite-gneiss-granite associations which is widespread in Nigeria. In southwestern Nigeria alone, such associations have been observed around Iwo, Akure, Idanre, Ado-Ekiti and Ikare, Ogbomoso, Abeokuta, Igbeti, Okene, and Igarra among others [12,13]. The migmatite-gneiss-granite association in Idanre form the focus of this research. This report therefore showcases the mineralogy and geochemistry of the rocks for the purpose of establishing their geochemical characteristics, geotectonic significance and origin. This is noteworthy because diligent literature search revealed previous research has neither reported or emphasized the interrelationship or petrogenetic affiliation of the migmatite-gneiss-granite basement in SW Nigeria.

Regional Geology and Tectonic Setting

Nigerian Basement Complex forms southern segment of the Pan-African orogenic belt of Neoproterozoic age [14]. It is situated between the Archean-Paleoproterozoic block of the West African craton in the west, Congo craton in the southeast, and the East Saharan block in the northeast [15,16]. The orogenic belt extends across the entire African continent into the Brasiliano orogen of South America [17-21]. The entire north-south trending orogenic belt which is also called the Trans Saharan fold belt is characterized

by high-grade metamorphism, early thrust-napple development, numerous granite intrusions and late orogen-parallel tectonics [17,22]. The belt is made of a northern section comprising Pharusian belt, LATEA micro continent and Eastern Hoggar (Figure 1) [23]. The southern part is exposed in an area known as the Benin-Nigeria Shield (The Dahomeyide) which comprise of several blocks amalgamated during oblique collision [24] and stretches from the eastern margin of the West African craton to the border of the Congo craton [22,24]. The Nigerian sector of the orogenic belt has been delineated into eastern and western terranes by a north-south trending lineament that has been recognized from remote sensing, but not studied in detail [15,27-31]. Evidence from the eastern and northern margins of West African craton indicates that the Pan-African mobile belt evolved by plate tectonics processes which involved the collision of the passive continental margin of the West-African craton and the active margin of the Pharusian belt (Tuareg shield) about 600 Ma [32-34]. The presence of ophiolites, accretionary prisms, island-arc magmatic suites, high-pressure metamorphic assemblages, basic to ultrabasic rocks (believed to be either remnants of mantle diapirs or a paleo-oceanic crust) as documented in the Pan-African belts, revealed ocean opening, followed by a subduction and collision-related evolution between 900 and 520 Ma [11]. Due to its geographical extent, the duo believed the Pan-African may not be a single orogeny, but several overlapping orogenic cycles related to the opening and closing of large oceanic realms as well as accretion and collision of buoyant ancient crustal blocks. Further south, in the Tuareg Shield of Algeria, Mali and Niger, several terranes with contrasting lithologies and origin have been recognized, and ocean closure during westward subduction produced a collision belt with Pan-African rocks, including oceanic crust tectonically interlayered with older basement. The latter were thrust westwards over the West African Craton and to the east over the LATEA super terrane to form a completely deformed composite crustal segment consisting of Archaean to Neoproterozoic assemblages [11]. The eastern Part of the belt consists of a high-grade granitoid-gneiss terrane of the Nigerian province, partly consisting of Paleoproterozoic rocks which were migmatized at 600 Ma. This deformation and metamorphism are considered to have resulted from oblique collision of the Nigerian shield with the West African Craton, followed by anatectic doming and wrench fault [11].

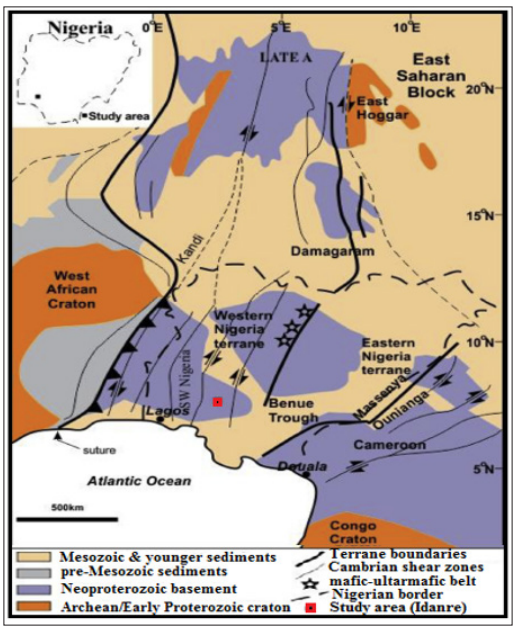

Figure 1: Geological Map of Pan African Mobile Belt East of West African Craton (modified from [14,22,24-28])

The tectonic evolution of the schist belt which forms a vital component of the Nigeria basement complex has been discussed [35-37]. Essentially, the evolution of the schist belts is related to a collision type orogeny in an eastward- dipping subduction zone during which initial crustal extension and continental rifting at the West African cratonic margin led to the formation of graben-like structures in western Nigeria and the subsequent deposition of rocks of the schist belts [38]. Closure of the ocean at the cratonic margin, about 600 Ma and crustal thickening led to deformation of the sediments, reactivation of the pre-existing rocks and emplacement of the Pan-African granites [39]. The Precambrian basement is exposed in two large areas, namely: northcentral and southwestern; and three smaller areas in the eastern side. These include, southeast (extension of the Bamenda Massif into Nigeria), northeastern (the Hawal Massif) and south-southeast (the Oban Massif) [40]. The older rocks in the basement are intruded by Pan-African syn-to-post-collisional plutons, which are more voluminous in the eastern terrane than the west [41]. Contemporaneous granitoid plutons are also found in the Pan-African belts to the west and north of Nigeria [41]. The basement complex of the western terrane (Figure 2), which forms a broader view of this study area, is dominated by Archaean migmatite gneisses, metasediments, Pan African granites and undeformed dykes [36]. The eastern terrane is characterized by high-grade migmatitic rocks that have Paleoproterozoic protoliths but were migmatized during the Neoproterozoic [27,28,30].

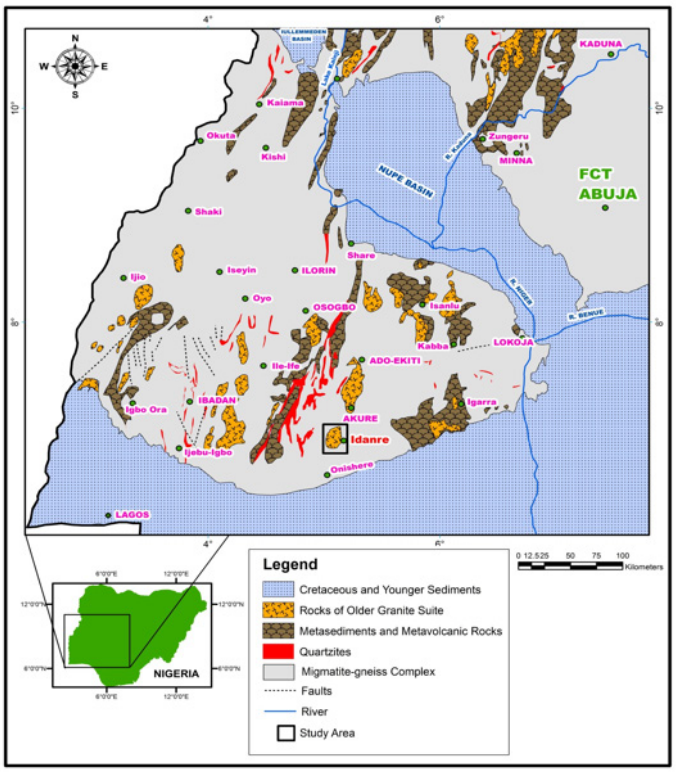

Figure 2: Geological Map of Southwestern Nigeria Showing Location of the Study Area

Field Relationship

The general landscape of the study area comprises of conical hills with heights ranging between 180 - 550 m above the mean sea level. Idanre area is higher than the surrounding rainforest zone of southwestern Nigeria which lies at approximately 200m above sea level [42]. The Idanre area consists of migmatite-gneiss, granite and charnockite, (Figure 3). Migmatite-gneiss complex across the country is generally Archaean to Paleoproterozoic age [43-46].

The Idanre migmatite-gneiss complex is made of three (migmatite, biotite-hornblende gneiss and banded gneiss) subunits.

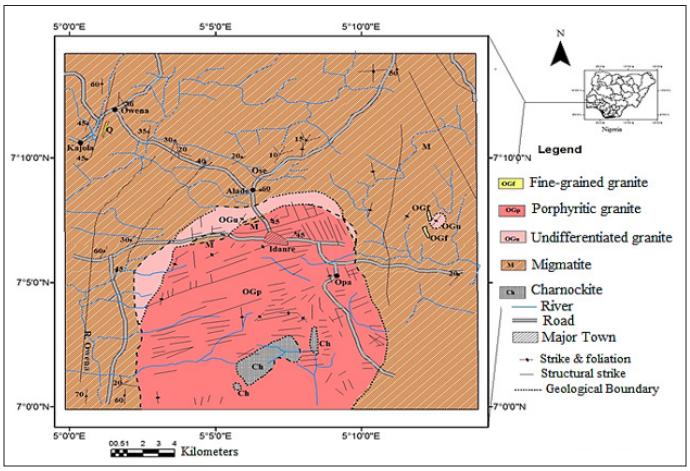

Figure 3: Geological Map of the Study Area Modified after Geological Survey Nigeria (1966)

Migmatite

Migmatite is the most extensive unit covering a greater percentage of the landmass of the study area. It is generally low-lying and most localities lacking rock exposures are believed to be underlain by migmatite. The migmatite in some places grade into gneiss, which is probably why previous authors considered the unit as one lithology. Believes the homogenizing effect of Pan-African orogeny led to metasomatism, dynamic metamorphism and magmatism which produced the various rock types depending on their original compositions [47]. The trio believes the problems associated with classifying the various shades of gneisses and migmatites in the basement complex are obvious. Strictly speaking, migmatite is the country rock in which the younger rocks have been emplaced [48]. The migmatitic rock was intensely involved in the Pan-African (600 Ma) mobile belt activity [49]. Idanre migmatite typically occurs as low-lying, fine-grained rock with complex fold structures. Fold geometry range from simple symmetrical types (Figure 4a) to shear folds and disharmonic ptygmatic folds. While the migmatitic rock show intense foliation in few localities, in other areas, the foliations become so indistinct that the bands are almost non-existing, leaving various indiscernible streaks of light and dark minerals. Other structural elements in the migmatite include fractures, joints, quartz vein intrusions and veinlets. The size of the quartz veins varies from tiny stringers of few millimeters width to those measuring up to 15cm in width. Quartz vein intrusions are commonly attributable to fracture fillings and by quartz injections.

Biotite-Hornblende Gneiss

Biotite-hornblende gneiss has a fine texture with faint banding. Abundant biotite flakes are sandwiched into planes that are distinct from the light-colored quartzo-feldspartic portions. The biotite-hornblende gneiss outcrops around Alade area are typically unique because their quartzo-feldspartic portions are restructured into discontinuous streaks of porphyroblasts of felsic aggregates having eugen structures (Figure 4b). The main structures in the rock are oriented in approximately N-S direction. The principal axis of foliation is aligned along a strike direction which ranges between N5oE and N18oE. Several quartz vein intrusions of varying dimensions crisscross each other on many outcrops.

Banded Gneiss

This unit occur in few localities as isolated low-lying masses which display conspicuous segregation into thin bands which are arranged into perfect patterns of alternating mafic and felsic minerals (Figure 4c). Outcrops of banded gneiss is intersected only in the southeastern part of the study area. In some localities, bands of leucocratic and melanocratic minerals are remarkable, while the lit-par-lit structure makes the rock typically unique. In few cases, the bands are so thin, whereas in others the laminae are thicker and more conspicuous. Remarkable structural attribute includes high-angle westerly dip values ranging from 72-81o.

Figure 4: (a) Migmatite Gneiss Outcrop near Alade-Idanre Road Junction Showing Wrinkled Surface which Display Complex Fold Styles; (b) Biotite-Hornblende Gneiss from the Study Area with Nebulitic Structures; (c) Banded Gneiss with Eugen Structure; (d) Porphyritic Granite Outcrops in the Heart of Idanre Town (e) Undifferentiated Older Granite with Whale Back Shape in Idanre; (f) Close View of the Phenocrysts of K-Feldspar in Idanre Porphyritic Granite

Granite

Towering granite inselbergs makes the study area a topographically unique terrane. Idanre town is located on a pediment surrounded by these dome-shaped, steep-sided and sparsely vegetated lofty hills which forms the charming scenic beauty of the town. The granite forms massive intrusive bodies within the migmatitic basement and occur in three textural forms. These are: (i) fine-medium grained biotite and biotite muscovite granite (OGf), which occur as small isolated units about 9km east of Alade-Idanre Road junction; (ii) coarse-porphyritic biotite and biotite-hornblende granite (OGp) which forms large masses around the built-up areas of the town; and (iii) the undifferentiated Older Granite (OGu) which rim the porphyritic granite in the northern part (Figure 3). The emplacement of the granite during the Pan-African orogenic activities which affected the entire terrane may have oriented the dominant structures of the basement rocks in a N-S direction.

Charnockite

The Idanre charnockite has a restricted occurrence, it is confined to the core of the porphyritic granite intrusions. The rock is

particularly unique due to its olive-green color, vitreous and greasy lustre, and a characteristic spheroidal weathering. Charnockite was believed to have diverse origins spanning metamorphic and igneous derivations and are only common in certain Precambrian basement areas of the country [50].

Mineralogical Features

Major rocks in the study area were subjected to optical analysis. Modes were determined by point counting and visual estimation. The data were collected using a Swift Model E point counter fitted with an automated stage. Samples examined are thin sections (approximately 30 mm x 40 mm area of rock) that had been prepared for microprobe analysis. Usually, the total counts were between 1500-2000 on each specimen. It is conducted in such a way that the whole surface of the thin section was covered. Minerals counted were alkali feldspar, plagioclase, quartz, biotite, hornblende, and accessory minerals (Table 1). Microscopic study shows that variations in texture, mineralogy and structure between hand specimen samples of migmatite, biotite-hornblende gneiss and banded gneiss are also reflected in the features observed in thin sections. Quartz, K-feldspar, biotite and hornblende are common to the three gneiss types. However, the percentage contribution of these constituents to the modal composition of each unit differs significantly. Minerals occurring as minor constituents are pyroxene, iron-oxide, apatite, zircon and garnet.

Migmatite Gneiss

Migmatite comprise quartz (42-47%; ca. 44.5%), feldspars (microcline, K-feldspar (22-28%; ca. 25%) and biotite (7-13%; ca. 10%) (Table 1). Quartz occurs as small crystals with well-defined outlines. It sometimes forms clusters of equigranular aggregates. Euhedral to subhedral porphyroblasts of quartz are sometimes surrounded by groundmass of mainly quartz and biotite. Quartz crystals are colorless, clear and lack any form of cleavage and constitutes approximately 45% of the rock in thin section (Figure 5a). Quartz grains show first order polarization color ranging between grey and white. Some of the quartz crystals show straight extinction while the few that are fractured and dislocated show undulose extinction. Feldspars are mainly albite with Carlsbad twins, biotite occurs as disoriented mineral laths.

Table 1 (Quartz); 2 (Feldspar); 3 (Biotite); 4 (Hornblende); 5 (Microcline); 6 (Mymekite); 7 (Orthoclase); 8 (Opaque); 9 (Albite); S (Sphene); P (Pyroxene); M (Muscovite)

Table 1: Modal Composition of the Basement Rocks of Idanre (in Volume Fractions)

Sample No	**1**	**2**	**Avg.**	**3**	**4**	**Avg.**	**5**	**6**	**Avg.**	**7**	**8**	**9**	**Avg.**
Rock type	**M**	**M**		**BHG**	**BHG**		**BG**	**BG**		**OGu**	**OGu**	**OGu**	
Minerals													
Quartz	42	47	44.5	43	45	44	39	43	41	49	45	52	48.7
Feldspar	28	22	25	25	21	23	23	18	20.5	14	11	8	11
Hornblende	6	9	7.5	12	9	10.5	5	2	3.5	10	14	12	12
Pyroxene	-	-	-				6	6	6	-	6	-	2
Biotite	13	7	10	18	15	16.5	12	13	12.5	13	9	13	12
Muscovite	6	8	7	2	4	3	7	10	8.5	8	8	7	7.3
Opaque	5	7	6	-	6	3	8	8	8	6	7	8	7
Total	100	100	100	100	100	100	100	100	100	100	100	100	100
Sample No		11	12	Avg.	13	14	15	Avg.	16	17	18	Avg.	
Rock type	OGp	OGp	OGp		OGf	OGf	OGf		CH	CH	CH		
Minerals													
Quartz	46	50	45	47	38	41	41	40	35	35	30	33.3	
Feldspar	28	20	24	24	26	23	20	23	26	21	25	24	
Hornblende	8	8	8	8	7	6	11	8					
Pyroxene		-	3	1	5	4	-	3	12	9	10	10.3	
Biotite	9	10	8	9	8	10	6	8	12	12	15	13	
Muscovite	4	6	8	6	9	5	7	7		5	4	3	
Opaque	5	6	4	5	7	11	12	10	15	10	10	11.7	
Others							3	1		8	6	4.7	
Total	100	100	100	100	100	100	100	100	100	100	100	100	

Note: Avg. (Average); M (migmatite); BHG (Biotite hornblende gneiss); BG (Banded gneiss); OGu (Undifferentiated Older granite); OGp (Porphyritic granite); OGf (Fine-grained granite); CH (Charnockite)

Granite

The main mineral assemblage in the granite unit are plagioclase, K-feldspar, microcline, quartz, biotite, hornblende and opaque phase. The undifferentiated granite (OGu) has average composition of quartz (48.7%), feldspar (11%), hornblende (12%), biotite (12%), muscovite (7.3%), and opaque (7%) (Table 1). Similarities in mineralogical composition between the porphyritic granite (OGp) and fine-grained granite (OGf) is indicated by comparable feldspar and hornblende contents (Table 1). The undifferentiated granite carries large crystals of hornblende that are charged with several inclusions of quartz and pyroxene that are randomly arranged within the enclosing crystals (Figure 5d). Biotite occurs as very large plates with characteristic greenish-brown color, it bears rounded grains of quartz. Few euhedral crystals of sphene with diamond-shaped rhombs are observed. In the porphyritic granite, some microcline crystals are so large that they almost occupy the entire stage. It has characteristic grid (cross-hatched) twinning and grey to brown color. Few quartz grains are interlayered into characteristic myrmekite structures (quartz feldspar intergrowth) (Figure 5e). In the porphyritic granite, orthoclase occurs as large euhedral crystals with diagnostic Carlsbad twins (Figure 5f), it has well-defined edges. Smaller grains of quartz and hornblende form supporting minerals in the interlocking structure. In the fine-grained granite, quartz occurs as pleochroic mineral with almost equidimensional grains exhibiting white and grey color (Figure 5g). Biotite forms small pinkish to greenish mineral laths scattered in a disoriented manner. Hornblende are chestnut brown to greenish in color and forms the main supporting mineral across the entire stage (Figure 5h). Plagioclase occurs as large subhedral to anhedral crystals, similar but equidimensional masses also occur in clusters. The clusters may represent early plagioclase which crystallized from melt. The K-feldspar is orthoclase with size ranging from 8 to 12 mm while large crystals of microcline exhibits grid twinning and sometimes take a significant percentage of the stage. Quartz occurs as anhedral grains with undulose extinction indicating strain. Cracks are commonly observed in the quartz grains but not in the adjacent feldspar. The higher crack densities in quartz compared to adjacent grains indicates that the initiation of microcracking is genetically related to internal stresses in the crystal. The deformation features in the quartz crystals probably developed during cooling and uplift of the granite magma. Biotite is the main mafic aggregates and occurs in two (green and brown) color varieties. The pleochroic scheme varies from dark-brown to green, and brown to yellowish brown. Sometimes the mineral show evidence of alteration to chlorite particularly at the margin. Biotite occurs as anhedral plates and are arranged such that their longer axis is aligned towards same direction. Few crystals measuring up to 5 mm long are seen. Biotite commonly encloses numerous small crystals of apatite and magnetite. Hornblende is commonly observed in the marginal facies.

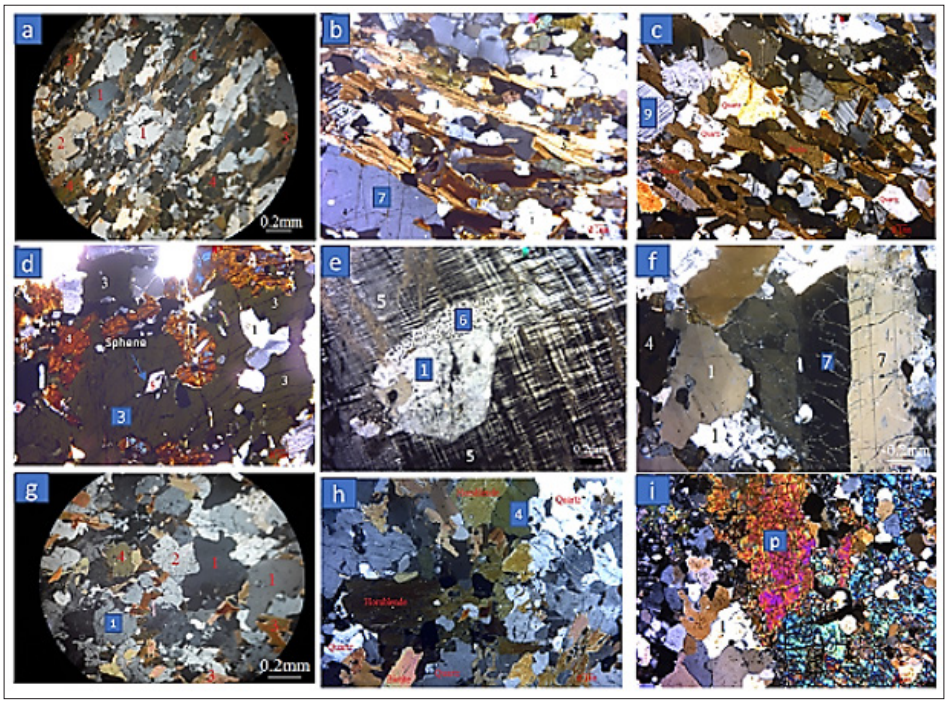

Figure 5: Photomicrograph (xpl) of the Rocks in the Study Area showing the Minerals Components (a) Migmatite; (b) Biotite-Hornblende Gneiss; (c) Banded Gneiss (d) Undifferentiated older Granite (e), (f) Porphyritic Granite; (g) Fine Grained Granite (h) Fine Grained Granite, (i) Large PYROXENE crystal

Charnockite

The charnockite comprises quartz (30-35%, ca. 33.3%), plagioclase (21-26%, ca. 24%), pyroxene (hyphersthene) (9-12%, ca. 10.3%), biotite (12-15%, ca. 13%), and muscovite (0-5%, ca. 3%) (Table 1). Large crystals of pyroxene with characteristic mesh texture are observed in the charnockite (Figure 5i). Other minerals in subordinate amounts are zircon and opaque. Many grains carried inclusions of quartz, while orthoclase is twinned according to albite law (Carlsbad twinning). Few crystals of orthoclase display distorted twinning and micro cracks which are evidences of stress. Hyphersthene shows mesh texture, while few muscovite flakes exhibit distorted cleavages. The hornblende crystals are probably formed because of secondary growth. Opaque minerals are mainly iron oxide.

Materials and Analytical Methods

Systematic geological mapping was undertaken adopting standard geological methods in the sampling techniques. Samples are collected

from wide geographical spread across the terrane and weathered samples are avoided as much as possible. Rock samples are collected from outcrop exposures using a sledgehammer. Eighteen fresh and wholesome representative samples comprising six (6) basement gneisses, nine (9) granite, and three (3) charnockite obtained from the Migmatite-Gneiss-Granite terrain of Idanre were used in the study. Samples weighing about 0.5 to 1 kg obtained during fieldwork were trimmed to remove any trace of weathering to obtain the cleanest samples. 8 cm^3 (2 cm x 2 cm x 2 cm) of each rock sample were dried at room temperature overnight and later pulverized. Glass fusion discs were used in the analysis of major elements. Each disc was prepared by using a mixture of approximately 0.5 g of 153-micron rock powder with 3.3 g of lithium borate flux in ratio 5.4321:1 flux: rock at 1150°C and the melt casted into 4 cm diameter aluminum plates. The resultant glass disc was then mounted on a backing disc for analysis. Powder pellets used in trace elements analysis were prepared by mixing 7 g of 53µ (micron) powder with 12 to 15 drops moviol binder solution (4 g Moviol + 10 ml ethanol + 50 ml distilled water). The resultant mixture was pressed into a 4cm disc under 5 tons pressure and dried before analysis following [51].

Geochemical analysis was carried out, major, trace and Rare Earth Element (REE) composition of the selected samples were determined. The Inductively Coupled Plasma Mass Spectrophotometer (ICP-MS) using Resonatcs 193NM Excimer Laser (Agilent 7700) and He-Ablation gas at 0.3L/min with a Carrier gas of 1L/min Ar+ 0.003L/min Nitrogen was adopted for the trace element; X-Ray Fluorescence (XRF) with Rh Tube was adopted for the major elements analysis. All geochemical analyses were undertaken at the commercial Laboratory, Ontario, Canada.

Major elements (SiO_2, Al_2O_3, Fe_2O_3, CaO, MgO, MnO, Na_2O, K_2O, TiO_2, P_2O_5) and trace elements (Ba, Ce, La, Nd, Nb, Pb, Rb, Sr, Th, Y and Zr) were determined. For the REE concentration, 0.25 g of powdered rock was weighed accurately into a graphite crucible and 2 g of Na_2O_2 was added. The mixture was then heated at 700oC for about an hour and then extracted and leached with water. The precipitation of hydrated oxide was dissolved with HNO_3 and analyzed using ICP-MS.

Result and Discussion

Compositional Features in Relation to other Nigeria Granites

The analytical result (Table 2) indicates that the average SiO_2 contents in the migmatite (ca. 65.18%), is higher than biotite-hornblende gneiss (ca. 60.85%) and banded gneiss (56.78%). Generally, the SiO_2 values range between 55.9%- 65.32% for all the gneisses. Mean Al_2O_3 content in the banded gneiss (17.22%) is higher than both migmatite (15.04%) and biotite-hornblende gneiss (14.76%). Average Fe_2O_3 content in banded gneiss (8.53%) and biotite-hornblende gneiss (8.53%) are comparable, but marginally higher than the migmatite gneiss (6.04%). Average SiO_2 content in the gneissic rocks from Idanre is comparable to garnet-silimanite gneiss (61.07%), migmatitic schists (57.33%-62.62%) but slightly lower than garnet-hornblende gneiss (65.9%) from the basement complex of Obudu areas in southeastern Nigeria; and migmatite (66.5-69.8%) from Ekiti area [53,54]. Similar trend though with slight variations occur in silica contents of other rock units. For instance, SiO_2 content in undifferentiated Older granite (OGu) (62.97–66.50%), porphyritic (OGp) (71.15-74.52%), the fine-grained granite (OGf) (63.60-67.90%) are all within the range (71.90-75.00%) reported from granites in Ekiti (74.25-76.52%), (73.52%-75.43%) [12] for porphyritic granite and medium grained granite from Ado-Ekiti area [55]. These values are also comparable to the Solli Hills granite (63.84-75.09%), Rahama amphibole-biotite granite (65.59-67.87%), Monzonite (62.92-67.79%) and Toro amphibole-biotite granite (65.74-69.18%) all from the basement complex of northcentral Nigeria [55]. The range of silica contents in Idanre charnockite (60.62-63.7%) is marginally lower than Ekiti charnockite 65.2-67.8% but comparable to Ado-Ekiti charnockite 58.60-64.33% and Obudu charnockite 53.63- 55.2% [12,53,54]. Al_2O_3 concentrations in the Idanre gneiss complex (14.76-17.6%), granite complex (12.29-18.71%) and associated charnockite (6.59–16.88 %) are comparable to similar rocks in the basement complex. Fe_2O_3 content in the Idanre granites (OGu: 2.33–6.56 %), (OGp: 2.74-3.2%) and (OGf: 3.98-6.00%) and charnockite (4.81–7.15 %) are expected for this kind of rocks. On average, the three oxides (SiO_2, Al_2O_3 and Fe_2O_3) constitute between 80–84% of the bulk chemical composition of the rock units in the study area. The relatively high concentration of these oxides is expected for this type of rocks and are in conformity with similar rocks from the basement complex of southwestern Nigeria.

Table 2: Analytical Result of the Major Basement Rocks in Idanre Area. (M1-M5) Migmatite-Gneiss, (OG) Granite (CH) Charnockite

Sample	M1	M2	M3	M4	M5	OGu	OGu	OGu	OGp	OGp	OGp	OGf	OGf	OGf	CH1	CH2	CH3
SiO2	65.32	65.04	60.85	57.66	55.9	66.5	62.97	64.2	73.76	74.52	71.15	63.6	66.0	67.9	63.53	60.62	63.70
Al2O3	14.98	15.1	14.76	16.83	17.6	14.27	18.71	17.89	12.68	12.29	13.82	15.4	14.4	15.1	16.59	16.61	16.88
Fe2O3	5.91	6.17	8.53	8.47	8.59	6.56	2.88	2.33	2.88	2.74	3.2	6.0	6.32	3.98	5.23	7.15	4.81
MgO	1.73	1.89	1.41	1.36	1.45	0.67	0.65	0.58	0.37	0.22	0.42	1.08	0.85	0.48	0.52	0.72	0.46
CaO	3.8	4.17	3.49	3.55	3.71	2.26	2.83	1.95	1.42	1.33	1.62	2.97	3.01	1.93	2.51	2.91	2.4
Na2O	3.03	3.18	3.05	3.58	3.81	3.07	4.05	3.11	2.67	2.83	2.95	3.13	3.55	3.25	3.66	3.72	3.81
K2O	3.92	3.17	5.25	5.64	5.83	4.95	6.51	8.4	5.29	4.87	5.75	5.74	3.9	6.15	6.41	6.19	6.43
TiO2	0.6	0.64	1.45	1.37	1.44	0.78	0.2	0.19	0.36	0.23	0.41	0.9	0.84	0.49	0.62	0.9	0.52
P2O5	0.17	0.18	0.47	0.34	0.33	0.23	0.08	0.11	0.08	0.04	0.1	0.31	0.27	0.14	0.14	0.21	0.12
MnO	0.09	0.09	0.12	0.1	0.11	0.07	0.04	0.04	0.03	0.03	0.03	0.07	0.07	0.04	0.09	0.13	0.08
LOI	0.2	0.1	0.2	0.3	0.4	0.3	0.6	0.5	0.2	0.7	0.3	0.4	0.4	0.3	0.6	0.3	0.4
Total	99.84	99.83	99.74	99.55	99.5	99.82	99.82	99.84	99.83	99.81	99.83	99.7	99.7	99.8	99.87	99.77	99.7
Ba	844	687	1567	3201	3054	1402	2622	3256	819	391	1057	1721	702	992	1295	1624	1525
Be	4	4	0.8	4	6	1	4	4	1	4	1	2	5	4	1	2	bdl
Cs	0.6	0.5	0.3	0.1	0.1	0.1	0.3	0.2	bdl	0.4	bdl	0.3	0.2	0.2	0.2	0.3	0.4
Ga	16	16.2	19.7	20.8	22.8	21.7	16.4	14.4	16.5	16.1	16.9	20	20.8	18.7	18.7	21.6	21.5
Hf	5.2	6.2	14.7	36.1	42.4	14.3	4.2	4.4	8.7	6.9	8.6	14.4	17.2	8.1	5.4	19	26.3

Nb	14.5	17	48	61.6	61.5	30.7	8.8	26.2	59	81.7	14.7	45.8	35.2	36	11	42.4	48.5
Rb	151.8	140.7	163.4	134.8	154.4	145.2	187.8	229.2	164.4	230.8	181.5	186	146	194	302.4	132.5	123.5
Sr	348.3	338.7	280.2	582.7	580.7	229.8	735	711.1	214.6	115.3	235.5	366	223	252	238.9	227.7	241.2
Ta	0.9	1	3.1	4.7	4.1	11.7	4.5	20.2	45.6	67.2	5.6	13.2	11.4	12.2	6.05	12.1	16.6
Th	32.4	36.2	17.7	3.5	5.2	20.5	9.9	18.5	25.5	111.5	29.5	18.4	59.5	29.4	16.7	27.6	20.2
U	1.9	2.1	1.6	0.9	1.1	1.7	0.9	1.3	1.9	11.8	1.2	1.4	2	1.5	2.1	2.9	2.3
Zr	182.2	217.7	616.5	1755	2025	615.1	150.3	171.3	371.2	244.6	336.8	619	741	354	789.1	1160	629.6
Y	31.7	35	49.5	48.6	50.3	35.5	21.1	17.2	18	20	18.2	43	49.2	22.1	29.2	36.1	22
Nb/Ta	16.11	17.00	15.48	13.69	15.0	2.62	1.96	1.29	1.29	1.21	2.63	3.47	3.08	2.95	1.82	3.50	2.92
La	58	59.9	105	134.5	137.4	61.5	62.7	103.2	138	200.9	154.8	142	344	161	97.7	136.7	124.2
Ce	108.5	107.3	206	285.8	285.9	167.3	111	180.5	244.1	360.9	267	282	622	284	186.3	266.1	213.8
Pr	11.38	11.59	22.56	33.99	33.03	14.37	12.6	16.88	22.62	33.57	25.07	29.9	59.1	27.6	19.66	28.23	21.22
Nd	41.5	43.1	82.2	131.2	122.3	52.4	43.6	53.4	71.5	99.3	79.5	106	186.5	88.5	73.5	103.8	75
Sm	7.24	6.94	14.12	21.69	19.99	10.24	7.37	7.27	9.29	13.1	9.85	16.72	25.17	12.29	11.44	15.96	9.84
Eu	1.45	1.38	3.04	4.86	4.45	2.35	2.34	2.31	1.8	1.14	1.89	2.74	2.38	2.28	3.3	3.24	3.31
Gd	6.22	6.63	12.23	16.37	14.79	9	5.38	5.26	5.89	7.52	6.56	12.5	17.09	8.52	9.38	12.05	7.32
Tb	0.91	1.01	1.81	2.07	1.91	1.36	0.78	0.68	0.73	0.92	0.79	1.71	2.13	1.05	1.14	1.57	0.86
Dy	5.35	6.01	9.75	11.25	10.12	7.24	4.31	3.49	4	4.61	3.9	9.34	10.73	5.23	6.25	7.95	4.56
Ho	1.09	1.27	1.92	1.88	1.82	1.39	0.72	0.64	0.6	0.74	0.66	1.61	1.92	0.87	1.13	1.43	0.8
Er	3.4	3.69	5.26	5.27	4.9	3.79	2.14	1.76	1.61	1.94	1.74	4.38	5.08	2.44	3.1	4.04	2.23
Tm	0.51	0.54	0.73	0.68	0.7	0.53	0.29	0.22	0.24	0.28	0.22	0.58	0.64	0.29	0.42	0.56	0.31
Yb	3.41	3.66	4.59	4.4	4.53	3.33	1.88	1.42	1.42	1.71	1.4	3.45	4.04	1.92	2.74	3.74	2.05
Lu	0.5	0.6	0.66	0.62	0.65	0.48	0.24	0.22	0.22	0.25	0.21	0.53	0.56	0.26	0.45	0.58	0.36

Geochemistry

The geochemical data was plotted on variation diagrams to establish the evolution trend of the rocks. The major elements Harker diagrams (Figure 6) show negative correlation with SiO_2. All the major oxides (Al_2O_3, MgO, CaO, Fe_2O_3, Na_2O, TiO_2 and P_2O_5) except K_2O apparently decreased with increasing SiO_2 content. The decreasing trend of most variation diagrams suggested fractionation of mafic minerals. Geochemical classification of granitic rocks is based upon three variables. These are FeOt/FeOt+MgO, the Modified alkali-lime index (MALI) (Na_2O+K_2O-CaO), and the aluminum saturation index (ASI) [Al/Ca-1.67P+Na+K]. The Fe-number distinguishes ferroan granitoids which manifest strong iron enrichment from magnesian granitoids which do not. The ferroan and magnesian granitoids can further be classified into alkalic, alkali-calcic, calc-alkalic, and calcic based on modified alkali-lime index (MALI) and subdivided based on ASI into peraluminous, metaluminous or peralkaline. Because alkalic rocks are not likely to be peraluminous, and calcic and calc- alkalic rocks are not likely to be peralkaline, The variation plot of FeOt/(FeOt + MgO) versus SiO_2 (Figure 7a) indicates the rock units are ferroan [56]. Ferroan (Fe-enriched) granites are closely associated with conditions of limited availability of H_2O and low oxygen fugacity during partial melting of their source rocks as well as the crystallization of anhydrous silicates [56]. On the other hand, magnesian granites are associated with relatively hydrous magmas and oxidizing differentiation trends [60]. It would therefore appear that these granitic rocks evolved under largely intermediate conditions with respect to these parameters. Na_2O+K_2O and CaO contents was used to classify the rocks geochemically using the Alkali-lime index, this is adapted in a plot of (modified alkali-lime index) Na_2O+K_2O-CaO versus SiO_2 diagram after (Figure7b) which categorized the rock units into alkali-calcic and calcic-alkali series [56,61]. Also, Al_2O_3/Na_2O+K_2O (ANK) versus Alumina Saturation Index (ASI) plot (Figure 7c) where ASI axis represents $Al/(CaO-1.67P_2O_5+Na_2O+K_2O)$ categorize the rocks as metaluminous (ACNK 0.84-1.02) [62]. A metaluminous rock is that in which ASI<1.0 and molecular Na_2O+K_2O<Al. In such rock, there is likely to be excess Ca after aluminum has been accommodated in the feldspars. As a result, metaluminous rocks contain calcic phases such as hornblende and augite but lack either muscovite or sodic ferromagnesian phases. Rocks with ASI >1.0 are corundum normative and are termed peraluminous, S-type, syn-collisional granitoids, continental collision granitoids, and muscovite-peraluminous granites [58,59,63-65]. This means that they have more Al than can be accommodated in feldspars and that they must have another aluminous phase present.

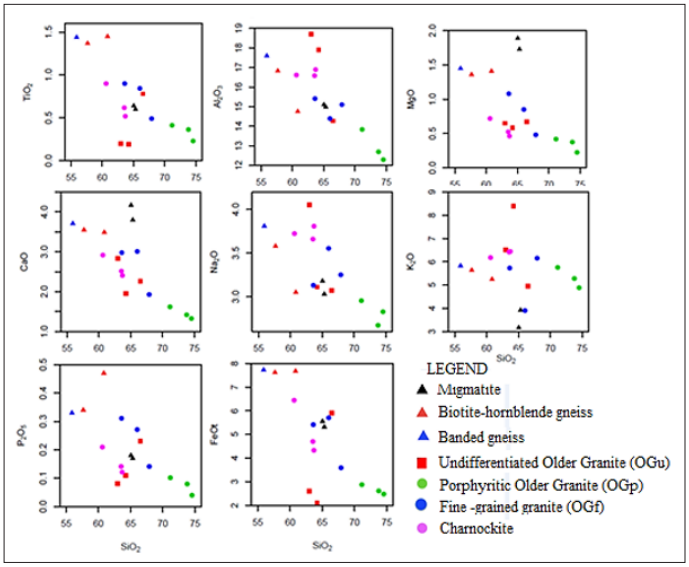

Figure 6: Major Elements Harker Diagrams for the Rocks in the Study Area

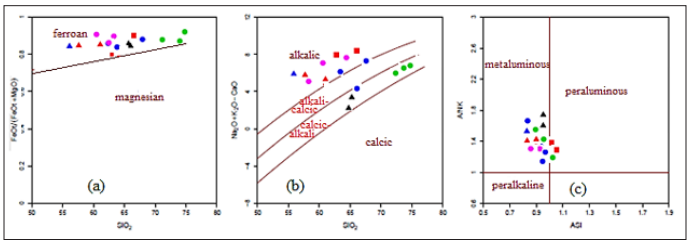

Figure 7: (a) $FeO^t/(FeO^t + MgO)$ Versus SiO_2 plot (after [56]) of Rocks in the Study Area (b) (Na_2O+K_2O)-CaO Versus SiO_2 plot for Subdivision of Granitoids According to the Modified Alkali-lime Index of [56]. (c) ANK Versus ASI plot (after [57-59]) for the Rocks in the Study Area. (symbols as in Figure 6)

The binary plot of Al_2O_3 versus MgO (Figure 8) after) shows that the samples fall in the orthogneiss field which means that the rock formations are largely derived from igneous ancestors [66].

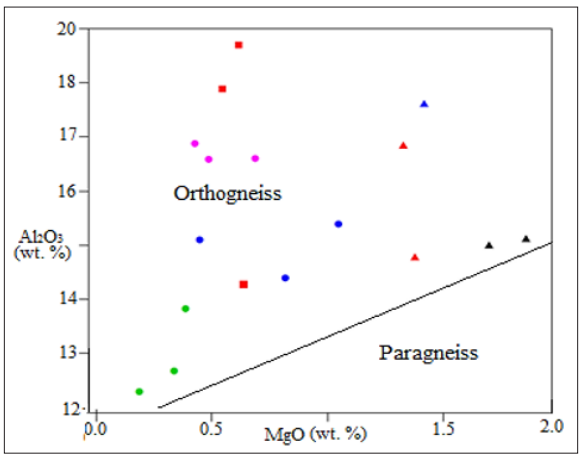

Figure 8: Al_2O_3 Versus MgO Discrimination Diagram (after [66]) (symbols as in Figure 6)

Generally, all the gneissic and granitic units are enriched with high alkaline contents ($Na_2O + K_2O$) ranging from 7.70 to 11.51 wt.% for the granite and 6.35 to 9.64 wt.% for the gneisses. The chemical classification and nomenclature of volcanic rocks using the total alkalis (Na_2O+K_2O) versus SiO_2 (TAS) diagram of, adapted by for plutonic rocks and (Figure 9) show that most of the rocks lie within the granite field [67-69]. K_2O versus SiO_2 diagram (Figure 10a) show all the samples plot in continental granophyre field indicating that some crustal materials were probably involved in the magma generation [70]. $(Na_2O+ K_2O)$-Fe_2O_3-MgO (AFM) Ternary diagram (Figure 10b) with the dividing lines (after) classifies the rocks as calc-alkaline series [71,72]. The ternary Ba-Rb-Sr diagram of (Figure 11) show the rocks plot extensively on anomalous granite field with few samples within granodiorite and quartz diorite fields [73].

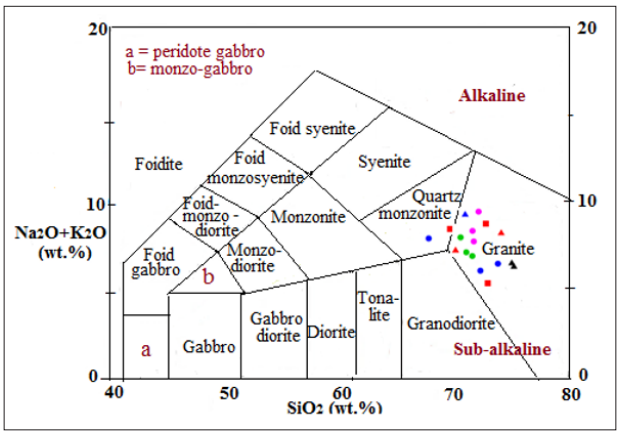

Figure 9: Total Alkali Versus Silica (TAS) Diagram [69] (Symbols as in Figure 6)

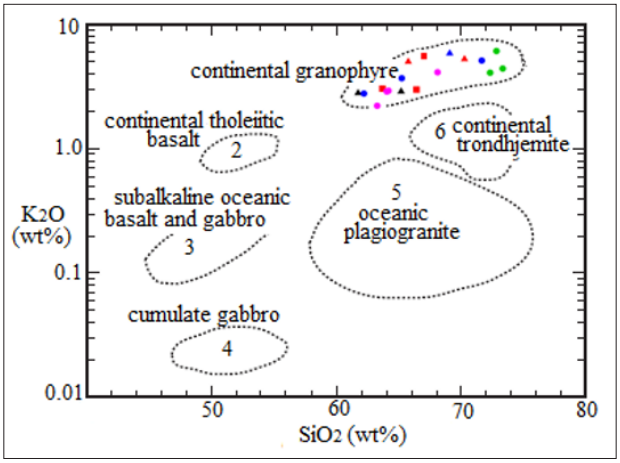

Figure 10: (a) K_2O Versus SiO_2 Diagram (after [70]) (symbols as in Figure 6)

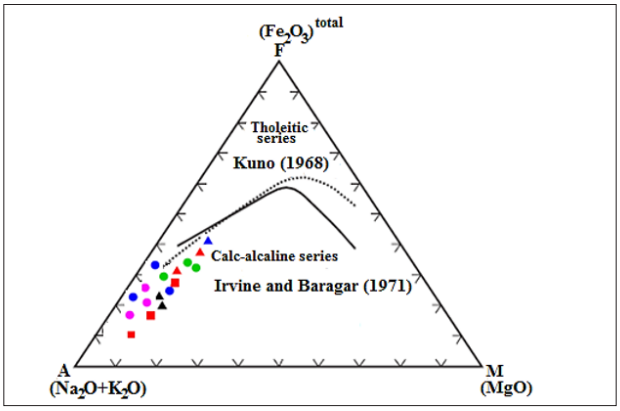

Figure 10: (b) AFM Ternary Diagram with the Dividing Lines After [71,72]. (Symbols as in Figure 6)

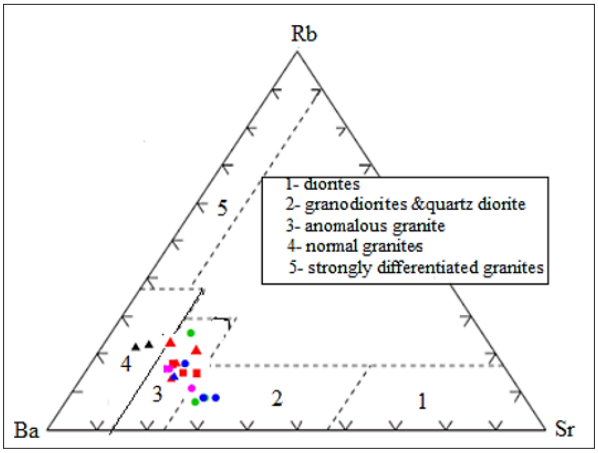

Figure 11: Ba-Sr-Rb Ternary Diagram of for the Rocks in the Study Area [73]. (Symbols as in Figure 6)

Trace element geochemistry (Table 2) indicates enrichment in Ba, Rb, Sr, Zr and Ce relative to other trace elements. Harker diagrams of trace elements (Figure 12) indicates that while Ba, Zr, Sr and Y shows negative correlation with SiO_2, Rb shows a positive relationship with increasing SiO_2 contents while La trend is indiscernible on the scatter diagram. This indicates that some of the trace elements probably behaved in a less mobile manner during the magmatic process or subsequent metamorphism. Indicate that Ti, Zr, Y and Nb are generally immobile during metamorphic processes [74]. Even though there appear no significant variation between the gneissic and granitic rocks in terms of Nb and Rb contents, a noticeable geochemical difference exists between their Ta contents. The gneisses contain lower Ta values (0.9-4.7 ppm) than the granite (4.5-67.2 ppm), consequently, Nb/Ta ratios vary between 13.69-17.00 ppm and 1.21-3.50 ppm respectively for the two rock types. The variation in Nb/Ta components may be attributed to either differences in age, mineralogy or composition between the gneiss and granite rock types. TiO_2 versus Zr plot (Figure 13) shows the different crystallizing options in the granite is controlled by some combination of crystallization of zircon + hornblende, zircon +sphene, zircon + magnetite+ biotite, and zircon + hornblende + sphene + magnetite.

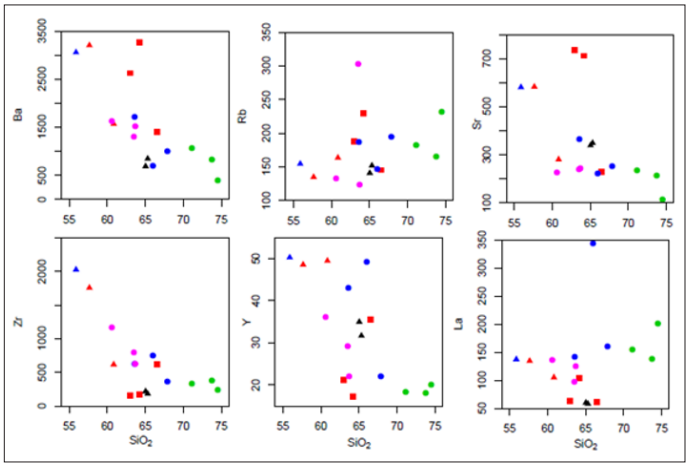

Figure 12: Trace Elements Harker Diagram for the Gneiss and Granitic Rocks (symbols as in Figure 6).

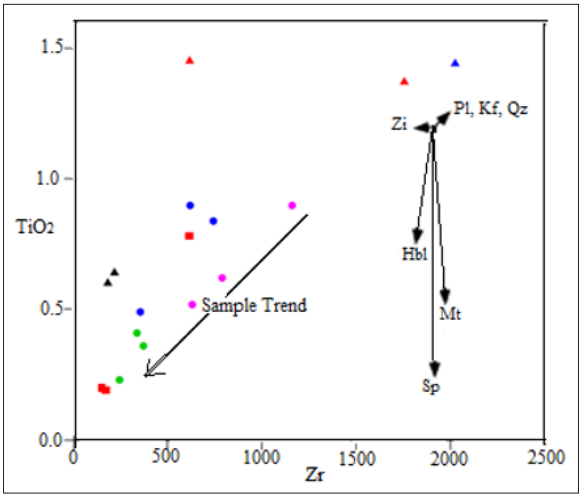

Figure13: TiO_2 versus Zr Plot of the Gneiss and Granite Rocks from the Study Area. Mineral Vectors Indicate Path Evolved Liquids for 15% of a Mineral Precipitating: Pl = Plagioclase; Kf = K-feldspar; Qz = quartz; Mt = magnetite; Sp = sphene; Hbl = hornblende; Zi = zircon.

The significant interest in the geochemistry of REE has come from the viewpoint that the observed degree of REE fractionation in rocks of granitic composition or mineral can be a pointer to its origin. The application of REE abundances to petrogenetic problems centered on the evolution of igneous rocks where such processes as partial melting of crustal or mantle materials, fractional crystallization and /or mixing of magmas are involved [75]. REE resources of granites are mostly associated with accessory minerals while some accessory minerals favour the LREE (e.g., allanite), others the HREE (e.g., zircon). REE elements from La to Lu were analyzed for the rock samples. REE concentration for the chondrite Leedy were used for normalization. The granite rock has average total REE 250-810 ppm (mean: 530 ppm) [76]. All the samples are enriched in light rare earth elements (LREE) and depleted in heavy rare earth elements (HREE). The LREE in the rock samples typically have 200 to 1010 times chondrite levels, whereas the HREE have 6 to 25 times chondrite levels (Figure 14). One of the most striking features of the REE distribution in the gneissic and granitic rocks is the similarity of both chondrite normalized profiles; they both show a family-like profile. Majority of the analyzed samples display similarities in their REE shape with each sample showing a negative Eu anomaly. Eu anomalies are usually generated by fractional crystallization or fusion of plagioclase feldspar, garnet, apatite, allanite, magnetite and possibly clinopyroxene and amphibole. The petrographic analyses however reflects this position. The presence of prominent Eu anomaly in the rocks indicates that plagioclase fractionation is an essential requirement in the development of the Idanre granitic series. On the primitive mantle normalized spider diagram (Figure 15), the granite samples show a strong depletion in Nb, P, Ti but Th and Ta enrichment, whereas the gneissic rocks show a profound Ta depletion [77].

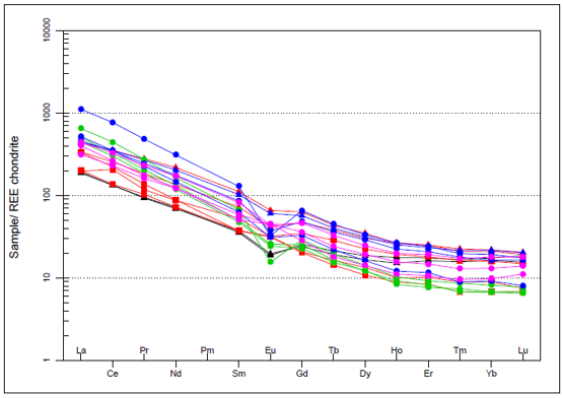

Figure 14: Chondrite Normalized REE Distribution Pattern of the Gneiss-Granite Rocks in the Study Area

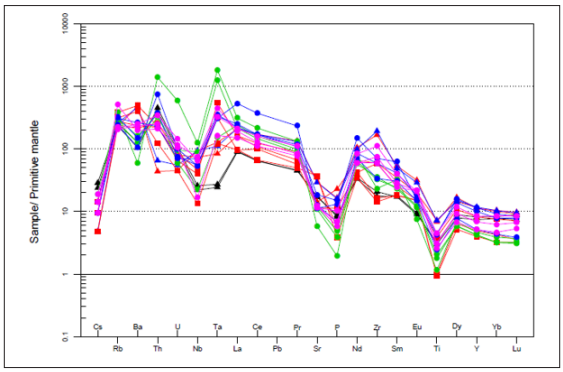

Figure 15: Primitive Mantle/Spider plot for the Gneiss-Granite Rocks from the Study Area

Rock Classification

Mineralogy of the granitic rock, especially the occurrence of sphene and hornblende suggest that they are of 'I' type. This is supported by ACNK (Al_2O_3/CaO+Na_2O+K_2O) values where all the granitic samples fell below ACNK=1.1 (Figure 16) and have increasing ACNK values with respect to increasing SiO2, all suggested that the granite magma originates from igneous source [62,78]. Na_2O versus K_2O diagram (Figure 17) showed that both the gneiss and granitoids samples plot in I- type domain also implying that the magma source is Igneous in origin. Evidence of I-type for the granite is further displayed on P_2O_5 versus SiO_2 plot (Figure 18) in which the main difference between the compositions that result from the crystal fractionation of felsic I and S type melts is that with increasing SiO_2, P_2O_5 decreases in I-type granite and increases in S type melts [79].

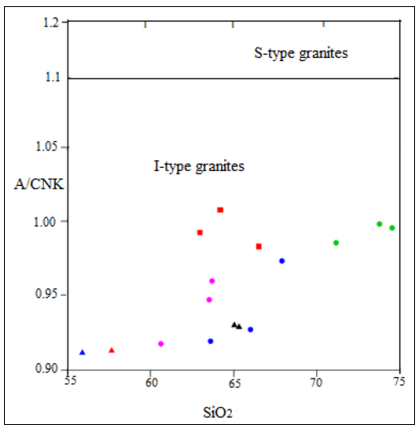

Figure 16: ACNK Versus SiO_2 plot for Gneiss-Granite Rocks of Idanre Area

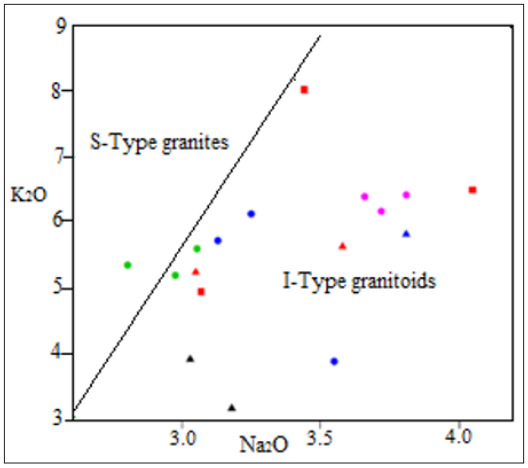

Figure 17: Na_2O Versus K_2O plot for the Gneiss and Granite Rocks from the Study Area (Symbols as in Figure 6).

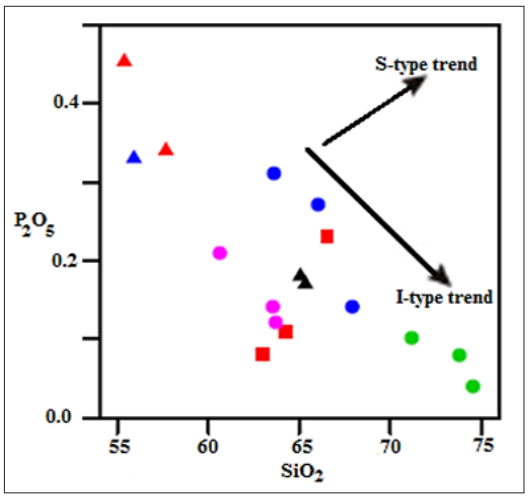

Figure 18: P_2O_5 Versus SiO_2 plot for Gneiss And granite Rocks from Idanre Area. The Arrow shows a Decreasing Trend for both Gneiss and Granitoid Samples (Symbols as in Figure 6).

Tectonic Implication

Showed that tectonic discrimination of the protolith of the migmatite-gneiss-granite rocks using the parameters R1 and R2 calculated from milli-cations proportions [80,81]. R1=4Si-11(Na+K)-2(Fe+Ti); R2= 6Ca +2Mg+Al can discriminate five granitic groups related to the tectono-magmatic divisions proposed by [82,83]. The diagram shows the rock plots in late orogenic to syn-collisional field (Figure 19). The different intrusive complexes are clearly distinguished according to their plate settings on well-established granite discrimination diagrams. Proposed that granites may be subdivided according to their intrusive settings into four main groups which are ocean ridge granites (ORG), volcanic arc granites (VAG), within plate granites (WPG) and collision granites (COLG) [64]. Discrimination of ORG, VAG, WPG and syn-COLG can be established effectively on Rb-Y-Nb and Rb-Yb-Ta space, particularly on projections of Y-Nb plots. Tectonic discrimination plot of Nb versus Y (Figure 20a), both granite samples as well as the gneissic country rock plot on Within Plate Granite (WPG) and Volcanic Arc+Syn-COLG (VAG+ Syn-COLG) granites fields [64]. This is further discriminated using the Rb versus Ta+Yb diagram (Figure 20b) where most samples plot inside the WPG while other samples clusters around the dividing line between the Syn-COLG and VAG fields [64]. Ta versus Yb discrimination diagram (Figure 20c), revealed all the samples fell on WPG and VAG but

with no representation in Syn-COLG and ORG fields [64]. Rb versus Y+Nb discrimination diagram (Figure 20d), indicated all the samples plot and clustered on the dividing line between VAG and WPG fields with no major representation on the Syn-COLG or ORG confirming the Ta versus Yb diagram [64].

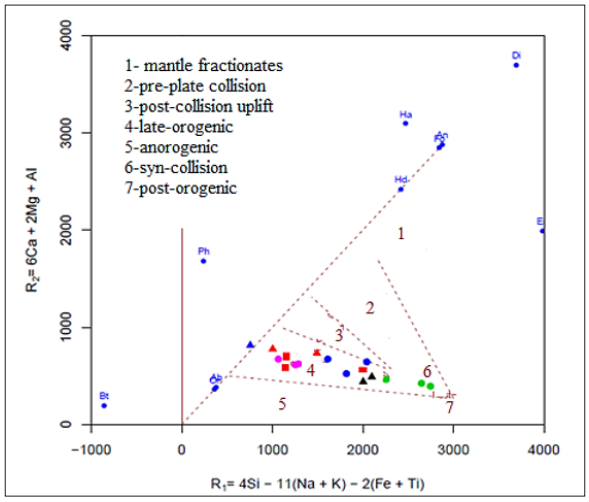

Figure 19: R1 vs R2 Diagram for the Migmatite-Gneiss and Granite Rocks in the Study Area

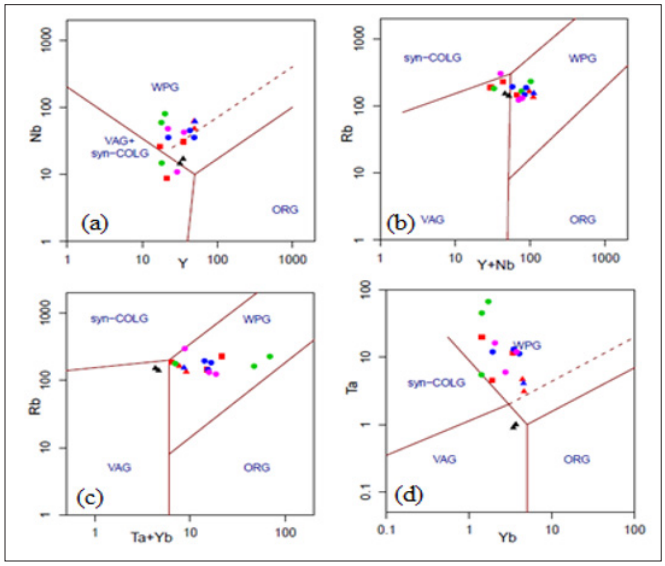

Figure 20: Tectonic Discrimination plots of (a) Nb Versus Y, (b) Rb Versus Y+Nb, (c) Rb Versus Ta +Yb, and (d) Ta Versus Yb for the Rocks in the Study Area (Symbols as in Figure 6)

Summary

Field geology indicates that granite in Migmatite-gneiss-granite belt of Nigeria occur as intrusive bodies in the form of fine-grained, porphyritic, and coarse-grained (undifferentiated) suites. Petrographic investigation reveals the gneiss is dominated by quartz, feldspar and biotite and hornblende; while the granite contain quartz, K-feldspar, microcline, biotite, hornblende, magnetite sphene and opaque magnetite. Despite slight petrographic differences between the two rock types, geochemical features of the migmatite-gneiss-granite rocks are comparable to similar rocks reported from other areas of the basement complex of Nigeria. Harker diagrams of major elements indicates fractionation of the mafic minerals. Compositionally, FeOt/(FeOt+MgO) versus SiO_2 variation plot classifies the migmatite-gneiss-granite rocks as ferroan type, Al_2O_3 versus MgO plot classifies them orthogneiss while total alkali (Na_2O+K_2O) versus SiO_2 (TAS) classified the rocks as granite. K_2O versus SiO_2 binary plot classifies the rock as continental granophyre. AFM [(Na_2O+K_2O)-Fe_2O_3-MgO] ternary diagram geochemically classifies the rock as calc-alkaline series. Al_2O_3+Na_2O+K_2O versus Alumina Saturation Index (ANK vs ASI) plot indicates ASI<1.0 showing the granite is metaluminous, while a decreasing trend in the P_2O_5 versus SiO_2 plot indicate I-type granitoids. Low ACNK values (<1.1), a decreasing trend on ACNK versus SiO_2 binary diagram indicates the rocks originates from partial melting of igneous protoliths. Na_2O versus K_2O variation diagram indicates both the gneiss and granite originate from a similar source. The similar shape for the chondrite normalized REE distribution for both migmatite-gneiss and granite reveal similar geochemical trends, all the samples exhibit negative Eu anomaly implying plagioclase fractionation. La/Sm versus Sm plot indicate the significance of partial melting in the genesis of the magma that formed the rocks. Tectonic discrimination using Nb versus Y and Rb versus Y+Nb shows the granite rocks were emplaced into within plate (WPG) environment. Similar geochemical trends in the migmatite-gneiss-granite association indicates the rocks are tectonically related and are all produced by partial melting as indicated on La/Sm versus La binary plot (Figure 21) [84-103].

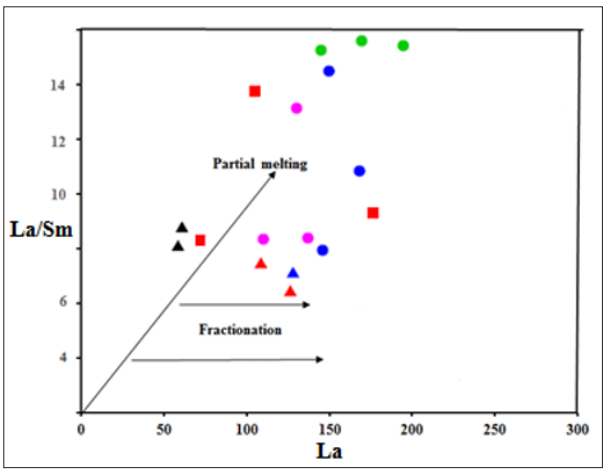

Figure 21: La/Sm Versus La plot for Gneiss and Granite Rocks in the Study Area (Symbols as in Figure 6).

Acknowledgements

We would like to express out thanks to the University of Malaya who provided the Faculty of Science Grant for the geochemical analysis. His Royal Majesty, The Oludanre of Idanre land, the High chiefs and the community at large is appreciated for the hospitality and for granting access to all nooks and corners of the study area for a successful geological mapping. The Tourism officer and all students who assisted during the fieldwork are acknowledged with thanks. The HOD and Dr. Fakolade of the Department of Mineral and Petroleum Resources Engineering Technology, Federal Polytechnic Ado-Ekiti are appreciated for allowing the Departmental cutting machine to be used.

References

1. Chapman JB, Ducea MN, DeCelles PG, Profeta L (2015) Tracking changes in crustal thickness during orogenic evolution with Sr/Y: an example from the North American Cordillera. Geology 43: 919-922.
2. Profeta L, Ducea MN, Chapman JB, Paterson SR, Gonzales SMH, et al. (2015) Quantifying crustal thickness over time in magmatic arcs. Scientific Reports 5: 17786.
3. Ducea MN, Saleeby JB, Bergantz G (2015) The architecture,

chemistry, and evolution of continental magmatic arcs. Annual Review of Earth and Planetary Sciences 43: 299-331.
4. Armstrong RL (1991) The persistent myth of crustal growth. Aust J Earth Sci 38: 613-640.
5. Goodwin MA (1991) Precambrian Geology: The Dynamic Evolution of the Continental Crust. Academic Press London 666.
6. Gorbatschev R, Bogdanova S (1993) Frontiers in the Baltic Shield. Precambrian Res 64: 03-21.
7. Rao YJB, Chetty TRK, Janardhan AS, Gopalan K (1996) Sm–Nd and Rb–Srages and P-T history of the Archean Sittampundi and Bhavani layered meta-anorthosite complexes in Cauvery shear zone, South India: evidence for Neoproterozoic reworking of Archean crust. Contrib Mineral Petrol 125: 237-250.
8. Wu FY, Jahn BM, Wilde S, Sun DY (2000) Phanerozoic crustal growth: U–Pb and Sr-Nd isotopic evidence from the granites in northeastern China. Tectonophysics 328: 89-113.
9. Belousova EA, Kostitsyn YA, Griffin WL, Begg GC, O'Reilly SY, et al. (2010) The growth of the continental crust: constraints from zircon Hf-isotope data. Lithos 119: 457-466.
10. Best MG (2003) Igneous and metamorphic petrology, 2nd ed. https://www.geokniga.org/bookfiles/geokniga-igneousandmetamorphicpetrologybymyrongbestz-liborg.pdf.
11. Kröner A, Stern RJ (2005) Pan-African Orogeny. Encyclopedia Geology 1: 1-12.
12. Oyinloye AO, Obasi RA (2006) Geology, Geochemistry and Geotectonic Setting of the Pan-African Granites and Charnockites Around Ado-Ekiti, Southwestern Nigeria. Pak J Sci Ind Res 49: 299-308.
13. Afolabi OA, Kolawole LF, Abimbola AF, Olatunji AS, Ajibade OM (2013) Preliminary study of the geology and structural trends of Lower Proterozoic basement rocks in Ogbomoso, SW Nigeria. Jour of Environment and Earth Science 3: 82-95.
14. Caby R, Dallmeyer RD (1989) Precambrian terranes of Benin-Nigeria and northeast Brazil and the Late Proterozoic South Atlantic fit. In: (Ed.), Terranes in the Circum-Atlantic Palaeozoic Orogens. Geological Society of America Special Paper 230: 145-158.
15. Woakes M, Rahaman MA, Ajibade AC (1987) Some metallogetic features of the Nigerian basement. Journal of African Earth Sciences 6: 655-644.
16. Odeyemi IB (1981) A review of the Orogenic events in the Precambrian basement of Nigeria, West Africa, Geol. Rundsch 70: 897-909.
17. Black R, Liegeois JP (1993) Cratons, mobile belts, alkaline rocks and continental lithospheric mantle: the Pan-African testimony. J Geol Soc Lond 150: 89-98.
18. Stern RJ (1994) Arc assembly and continental collision in the Neoproterozoic East African orogeny-implications for the consolidation of Gondwana. Annual Reviews of Earth and Planetary Sciences 22: 319-351.
19. Castaing C, Feybesse LL, Thieblemont D, Triboulet C, Chevremont P (1994) Palaeogeo-graphical reconstructions of the Pan-African/Brasiliano orogen: closure of an oceanic domain or intracontinental convergence between major blocks? Precambrian Research 69: 327-344.
20. Jacobs J, Thomas RJ (2004) Himalayan-type indenter-escape tectonics model for the southern part of the late Neoproterozoic-early Palaeozoic East African-Antartic Orogen. Geology 32: 721-724.
21. De Wit MJ, Stankiewicz J, Reeves C, Pankhurst RJ, Trouw RAJ, et al. (2008) Restoring Pan-African-Brasiliano connections: more Gondwana control, less trans-Atlantic corruption. In: (Eds.), Pre-Cenozoic Correlations across the South Atlantic Region. The Geological Society, London 399-412.
22. Adetunji A, Olarewaju VO, Ocan OO, Ganev VY, Macheva L (2016) Geochemistry and U-Pb zircon geochronology of the pegmatites in Ede area, southwestern Nigeria: A newly discovered oldest Pan African rock in southwestern Nigeria. Jour of Afr Earth Sci 115: 177-190.
23. Liégeois JP, Latouche L, Boughrara M, Navez J, Guiraud M (2003) The LATEA metacraton (Central Hoggar, Tuareg shield, Algeria): behavior of an old passive margin during the Pan- African orogeny. Jour Afr Earth Sci 37: 161-190.
24. Ajibade AC, Wright JB (1989) The Togo Benin Nigeria shield: evidence of crustal aggregation in the Pan African belt. Tectonophysics 165: 125-129.
25. Black R, Latouche L, Liegeois JP, Caby R, Bertrand JM (1994) Pan African displaced terranes in the Tuareg shield (central Sahara). Geology 22: 641-644.
26. Liégeois JP, Black R, Navez J, Latouche L (1994) Early and late Pan African orogenies in the Air assembly of terranes (Tuareg shield, Niger). Precambrian Res 67: 59-88.
27. Ferré EC, Deleris J, Bouchez JL, Lar AU, Peucat JJ (1996) The Pan African reactivation of Eburnean and Archaean provinces in Nigeria: a structural and isotopic data. Journal of the Geological Society of London 153: 719-728.
28. Ferré EC, Gleizes G, Caby R (2002) Obliquely convergent tectonics and granite emplacement in the Trans-Saharan belt of Eastern Nigeria: a synthesis. Precambrian Research 114: 199-219.
29. Fitches WR, Ajibade AC, Egbuniwe IG, Holt RW, Wright JB (1985) Late Proterozoic schist belts and plutonism in NW Nigeria. Journal of the Geological Society of London 142: 319-337.
30. Ajibade AC, Woakes M, Rahaman MA (1987) Proterozoic crustal development in the Pan-African Regime of Nigeria. https://agupubs.onlinelibrary.wiley.com/doi/10.1029/GD017p0259.
31. Ananaba SE, Ajakaiye DE (1987) Evidence of tectonic control of mineralization in Nigeria from lineament density analysis. A Landsat Study. International Journal of Remote Sensing 8: 1445-1452.
32. Burke KC, Dewey JF, Dessauvagie TFJ, Whiteman AJ (1972) Orogeny in Africa. In: (Eds.) African Geology Univ. Ibadan Geol Dept 583-608.
33. Leblanc M (1981) The late Proterozoic ophiolites of Bon Azzer (Morocco): evidence for Pan-African plate tectonics. In: Kroner, A., (Ed.), Precambrian plate tectonics, Elsevier Amsterdam 435-451.
34. Caby R, Betrand JML, Black R, Kroner A (1981) Pan-African Ocean closure and continental collision in the Hoggar-Iforas segment, central Sahara. In: (ed.) Precambrian plate tectonics, Elsevier Amsterdam 407-437.
35. Ajibade AC, Fitches WR, Wright JB (1979) The Zungeru mylonites, Nigeria. The recognition of a major tectonic unit. Rev. Geol Dyn Geogr Physique 21: 259-263.
36. Rahaman MA, Ajayi TR, Oshin IO, Asubiojo FO (1988) Trace element geochemistry and geotectonic setting of Ile-Ife schist belts. Precambrian Geol of Nigeria GSN pub Kaduna 241-256.
37. Elueze AA (1988) Geology of the Precambrian schist belt in Ilesha area, southwestern Nigeria. Prec Geol Nig Publication of the Geological Survey of Nigeria 2: 77-82.
38. Elueze AA (1992) Rift system for Proterozoic schist belts in Nigeria. Tectonophysics 209: 167-169.
39. McCurry P (1976) The Geology of the Precambrian to Lower

Palaeozoic rocks of northern Nigeria. https://www.scirp.org/reference/referencespapers?referenceid=1869377.
40. Obiora SC (2005) Field descriptions of hard rocks with examples from the Nigerian Basement Complex (1st edition). Snap Press Nig. Ltd, Enugu. 14.
41. Goodenough KM, Lusty PAJ, Roberts NMW, Key RM, Garba A (2014) Post-collisional Pan-African granitoids and rare metal pegmatites in western Nigeria: Age, petrogenesis, and the pegmatite conundrum. Lithos 200: 22-34.
42. Ige O, Adeyemi C, Ogunfolakan A, Ayansola A, Olayemi A, et al. (2011) An Inventory of the Geological, Biological and Cultural Resources on Ufe-Oke Hill, Idanre, southwestern Nigeria. Natural Resources 2: 180-190.
43. Dada SS (1989) Evolution de la croute continental au Nord Nigeria: apport de la geochimie de la geochronologic U-Pb et des traceurs isotopiques Sr, Nd et Pb. Univ Sci Tech Languedoc Montpellier 194.
44. Dada SS (1998) Crust-forming ages and Proterozoic crustal evolution in Nigeria: a reappraisal of current interpretations. Precambrian Res 87: 65-74.
45. Ekwueme BN, Kröner A (1992) Preliminary zircon evaporation ages from migmatitic gneisses in Kaduna, northern Nigeria: evidence for an early Archaean (Pre-Leonian) event in the Nigerian basement complex. In: IGCP 280 International Conference, Salvador, Brazil.
46. Annor AE (1995) U-Pb Zircon Age for Kabba-Okene Grano-diorite Gneiss: Implication for Nigeria's Basement Chronology. Africa Geoscience Reviews 2: 101-105.
47. Oluyide PO, Nwajide CS, Oni AO (1998) The geology of the Ilorin area. In: Geological Survey of Nigeria Bull 42: 84.
48. De Swardt AMJ (1953) The geology of the country around Ilesha: Bulletin. GSN 23: 54.
49. Elueze AA (1982) Geochemistry of the Ilesha granite gneiss in the basement complex of southwestern Nigeria. Precambrian research 19: 167-177.
50. Kilpatrick JA, Ellis DJ (1992) C-type magmas: Igneous charnockites and their extrusive equivalents. Transactions of the Royal Society of Edinburg- Earth Sciences83: 155-164.
51. Philpotts AR (2003) Petrography of igneous and metamorphic rocks. Waveland Press Inc. Prospect Heights, Illinois, USA. https://faculty.ksu.edu.sa/sites/default/files/ebooksclub.org__Petrography_of_Igneous_and_Metamorphic_Rocks_0.pdf.
52. Ghani AA, Yusoff I, Amir Hassan MH, Ramli R (2013b) Geochemical study of volcanic and associated granitic rocks from Endau Rompin, Johor, Peninsular Malaysia. Jour Earth Syst Sci 122: 65-78.
53. Ekwueme BN, Kröner A (2006) Single zircon ages of migmatitic gneisses and granulites in the Obudu Plateau: Timing of granulite-facies metamorphism in southeastern Nigeria. Journal of Africa Earth Sciences 44: 459-469.
54. Talabi AO (2013) Mineralogical and chemical characterization of major basement rocks in Ekiti State, SW-Nigeria. RMZ M&G 60: 73-86.
55. Ferré EC, Caby R, Peucat JJ, Capdevila R, Monie P (1998) Pan-African, post-collisional, ferro-potassic granite and quartz-monzonite plutons of Eastern Nigeria. Lithos 45: 225-279.
56. Frost BR, Barnes CG, Collins WJ, Arculus RJ, Ellis DJ, et al. (2001) A geochemical classification for granitic rocks. Journal of Petrology 42: 2033-2048.
57. Zen E (1986) Aluminum enrichment in silicate melts by fractional crystallization: some mineralogic and petrographic constraints. Journal of Petrology 27: 1095-1117.
58. Chappell BW, White AJR (1974) Two contrasting granite types. Pacific Geology 8: 173-174.
59. Maniar PD, Piccoli PM (1989) Tectonic discrimination of granitoids. Geological Society of America Bulletin 101: 635-643.
60. Frost BR, Lindsley DH (1991) The occurrence of Fe-Ti oxides in igneous rocks. In: Lindsley DH (ed.) Oxide Minerals: Petrologic and magnetic significance, Mineralogical Society of America. Reviews in Mineralogy 25: 433-486.
61. Peacock MA (1931) Classification of Igneous rock series. Jour of Geol 39: 54-67.
62. Shand SJ (1943) Eruptive rocks, 2nd ed. (London: T. Murby and Company) 444.
63. Zen E (1988) Phase relations of peraluminous granitic rocks and their petrogenetic implications. Annual Review of Earth and Planetary Sciences 16: 21-52.
64. Pearce JA, Harris NBW, Tindle AG (1984) Trace element discrimination diagrams for the tectonic interpretation of granitic rocks. Jour of Petrology 25: 956-983.
65. Barbarin B (1999) A review of the relationships between granitoid types, their origins and their geodynamic environments. Lithos 46: 605-626.
66. Marc D (1992) Granites and rhyolites from the northwestern USA: temporal variation in magmatic processes and relations to tectonic setting. Transactions of the Royal Society of Edinburgh Earth Sciences 83: 51-64.
67. Le Bas MJ, Le Maitre RW, Streickeisen A, Zanettin B (1986) A chemical classification of volcanic rocks based on the total alkali-silica diagram. Jour Petrol 27: 745-750.
68. Le Maitre RW (2002) Igneous rocks, a classification and glossary of terms; Recommendations of the International Union of Geological Sciences Sub-commission on the Systematics of Igneous Rocks. https://www.cambridge.org/core/books/igneous-rocks-a-classification-and-glossary-of-terms/7F458E82BF81BF6A011CEA0D41DE9311.
69. Middlemost EAK (1994) Naming Materials in the Magma/Igneous Rock System. Earth-Science Reviews 37: 215-244.
70. Coleman RG, Peterman ZE (1975) Oceanic plagiogranite. Journal of Geophysical Research 80: 1099-1108.
71. Kuno H, Hess HH, Poldervaart A, (1968) Differentiation of basalt magmas. In: (Eds.), Basalts: The Poldervaart Treatise on Rocks of Basaltic Composition. Wiley Interscience, New York 2: 623-688.
72. Irvine TN, Baragar WRA (1971) A guide to the geochemical classification of the common volcanic rocks. Canadian Jour of Earth Sciences 8: 523-548.
73. El Bouseily AM, El Sokkary AA (1975) The relation between Rb, Ba and Sr in granitic rocks. Chemical Geology 16: 207-219.
74. Winchester JA, Floyd PA (1977) Geochemical discrimination of different magma series and their differentiation products using immobile elements. Chem Geol 20: 325-343.
75. Clark AM, Henderson P (1984) Mineralogy of the Rare Earth Elements- Chapter 2; In: Developments in Geochemistry and Rare Earth Element Geochemistry. (Ed.) Elsevier Science Pub Comp Inc 2.
76. Masuda A, Nakamura N, Tanaka T (1973) Fine structures of mutually normalized rare-earth patterns of chondrites; Geochem. Cosmochim Acta 38: 239-248.
77. Sun SS, McDonough WF (1989) Chemical and isotopic systematics of oceanic basalts: Implications for mantle composition and processes. Geol Soc London Spec Pub 42: 313-345.
78. Chappell BW, White AJR (1992) I- and S-type granites in the Lachlan fold belt. Transactions of the Royal Society

Edinburgh: Earth Sciences 83: 01-26.
79. Chappell BW (1999) Aluminum saturation in I- and S-type granites and characterization of fractionated haplogranites. Lithos 46: 535-551.
80. Batchelor RA, Bowden P (1985) Petrogenetic interpretation of granitoid rock series using multicationic parameters. Chemical Geology 48: 43-55.
81. De la Roche H, Leterrier J, Grande Claude P, Marchal M (1980) A classification of volcanic and plutonic rocks using R1-R2 diagrams and major elements analyses-its relationship and current nomenclature. Chem Geol 29: 183-210.
82. Pitcher WS (1979) The nature, ascent and emplacement of granitic magmas. Jour Geol Soc London 136: 627-662.
83. Pitcher WS, Hsu K (1983) Granite type and tectonic environment; In: Mountain building processes. (ed.) (Lond Acad Press) 19-40.
84. Akinola OO, Okunlola OA (2014) Compositional characteristics and petrogenetic features of metasediments of Ijero-Ekiti area, southwestern Nigeria. RMZ M&G 61: 221-230.
85. Arthaud MH, Caby R, Fuck RA, Dantas EL, Parente CV, et al. (2008) Geology of the northern Borborema Province, NE Brazil, and its correlation with Nigeria, NW Africa. In: (Eds.) West Gondwana: Pre-Cenozoic Correlations Across the South Atlantic Region. Geological Society London Special Publication 294: 49-67.
86. Bruguier O, Dada SS, Lancelot JR (1994) Early Archaean component (>3.5 Ga) within a 3.05 Ga orthogneiss from northern Nigeria: U-Pb zircon evidence. Earth Planet Sci Lett 125: 89-103.
87. Dada SS, Brique I, Birck JL (1998) Primordial crustal growth in northern Nigeria; preliminary Rb-Sr and Sm-Nd constraint from Kaduna migmatite gneiss complex. Jour of Min Geol 34: 1-6.
88. Dada SS, Tubosun IA, Lancelot JR, Lar AU (1993) Late Archaean U-Pb age for the reactivated basement of northern Nigeria. Jour Afr Earth Sci 16: 405-412.
89. Dada SS, Pankhurst RJ, Trouw RAJ, Brito Neves BB, De Wit MJ (2008) Proterozoic evolution of the Nigeria-Boborema province. In: (Eds.), Geological Society of London Special publication 294: 121-136.
90. Elueze AA (1981a) Petrographic studies of metabasic rocks and metaultramafites in relation to mineralization in Nigerian schist belts. Jour Min and Geol 18: 31-36.
91. (1966) GSN Geological Survey of Nigeria, Geological Map of Akure, SW Nigeria. https://ngsa.gov.ng/.
92. Jacobson REE, Snelling NJ, Truswell JF (1963) Age determination in geology of Nigeria with special references to older and younger Granites. Overseas Geol Miner Resour Lond 9: 108-188.
93. Matheis G, Caen Vachette M (1983) Rb-Sr isotopic study of rare metal bearing and barren pegmatites in the Pan African reactivation zone of Nigeria. J Afr Earth Sci 1: 35-40.
94. Okeke PO, Meju M A (1985) Chemical evidence for the metasedimentary origin of Igarra Supracrustal rocks, SW Nigeria. Jour Mining and Geol 22: 97-104.
95. Okonkwo CT, Winchester JA (1996) Geochemistry and Geotectonic Setting of Precambrian Amphibolites and Granitic Gneisses in the Jebba Area, Southwestern Nige-ria. Journal of Mining and Geology 32: 11-18.
96. Okunlola OA, Adeigbe OC, Oluwatoke OO (2009) Compositional and petrogenetic features of schistose rocks of Ibadan area. Earth Science Res Jour 13: 29-43.
97. Okunlola OA (2003) Petrochemical and petrogenetic characteristics of metasedimentary rocks of Lokoja-Jakura Schist belt, Central Nigeria. Jour of Mining and Geology 39: 21-28.
98. Oversby VM (1975) Lead isotope study of aplites from the Precambrian rocks near Ibadan, southwestern Nigeria. Earth Planet Sci Lett 27: 177-180.
99. Rahaman MA, Tubosun IA, Lancelot JR (1991) U-Pb Geochronology of Potassic Syenites from Southwestern Nigeria and the timing of deformational events during the Pan-African Orogeny. Jour African Earth Sci 13: 387-395.
100. Rahaman MA, Emofurieta WO, Caen vachette M (1983) The potassic granites of Igbeti area: further evidence of the polycyclic evolution of the Pan-African belt in Southwestern Nigeria. Prec Res 22: 75-92.
101. Rahaman MA, Oluyide PO, Mbonu WC, Ogezi AE, Egbuniwe IG, et al. (1988) Recent advances in the study of the basement complex of Nigeria. In: (Eds.), Precambrian Geology of Nigeria, Geological Survey of Nigeria Special Publication 11-41.
102. Snelling NJ (1966) Geochronology. In Overseas Geological Survey Annual Report. HMSO, London.
103. Tubosun IA, Lancelot JR, Rahaman MA, Ocan OO (1984) U-Pb Pan-African ages of two charnockite-granite association from southwestern Nigeria. Contrib Mineral Petrol 88: 188-195.